Olfactory neurons expressing transient receptor potential channel M5 (TRPM5) are involved in sensing semiochemicals

Weihong Lin*, Robert Margolskee†, Gerald Donnert‡, Stefan W. Hell‡, and Diego Restrepo§¶

*Department of Biological Sciences, University of Maryland Baltimore County, Baltimore, MD 21250; †Department of Neuroscience, Mount Sinai School of Medicine, New York, NY 10029; ‡Department of Biophotonics, Max Planck Institute for Biophysical Chemistry, 37070 Göttingen, Germany; and §Department of Cell and Developmental Biology, Neuroscience Program, and Rocky Mountain Taste and Smell Center, University of Colorado at Denver and Health Sciences Center, Aurora, CO 80045

Edited by Linda M. Bartoshuk, University of Florida, Gainesville, FL, and approved December 13, 2006 (received for review November 17, 2006)

Olfactory sensory neurons (OSNs) in the main olfactory epithelium respond to environmental odorants. Recent studies reveal that these OSNs also respond to semiochemicals such as pheromones and that main olfactory input modulates animal reproduction, but the transduction mechanism for these chemosignals is not fully understood. Previously, we determined that responses to putative pheromones in the main olfactory system were reduced but not eliminated in mice defective for the canonical cAMP transduction pathway, and we suggested, on the basis of pharmacology, an involvement of phospholipase C. In the present study, we find that a downstream signaling component of the phospholipase C pathway, the transient receptor potential channel M5 (TRPM5), is coexpressed with the cyclic nucleotide-gated channel subunit A2 in a subset of mature OSNs. These neurons project axons primarily to the ventral olfactory bulb, where information from urine and other socially relevant signals is processed. We find that these chemosignals activate a subset of glomeruli targeted by TRPM5-expressing OSNs. Our data indicate that TRPM5-expressing OSNs that project axons to glomeruli in the ventral area of the main olfactory bulb are involved in processing of information from semiochemicals.

signal transduction | pheromone | stimulated emission depletion (STED) microscopy

The olfactory system perceives not only odorants that convey information on the environment but also semiochemicals (chemicals involved in animal communication, from the Greek *semeion* for "sign"), including pheromones (1–4). A key step in transmission of information is activation of the canonical cAMP signaling pathway by binding of odorants to olfactory receptors, resulting in influx of Ca^{2+} through a cyclic nucleotide-gated (CNG) channel and subsequent depolarization (5, 6). Targeted disruption of elements of the cAMP pathway, including the CNG channel subunit A2 (CNGA2) (7), the G protein G_{olf} (8), or adenylyl cyclase (AC) III (9), result in severe deficit of odorant-evoked responses to many odorants, demonstrating the dominant role of the cAMP pathway.

Semiochemicals, such as pheromones, social attractants, and major histocompatibility complex (MHC)-related odorants, signal social and sexual status, genetic makeup, and species identity important for the survival of the individual and the species (1, 10–13). Recent studies indicate that both the main olfactory epithelium (MOE) and olfactory bulbs respond to these chemosignals (14, 15). Consistent with these findings, sensory information from the main olfactory bulb projects to areas in the hypothalamus housing neurons that produce gonadotropin-releasing hormone and plays an important role in reproduction (16, 17). Further, a class of chemosensory receptors that recognize social amines found in urine have been identified recently in the MOE (18). Thus, it now is clear that the main olfactory system is involved in detection of semiochemicals and that the cAMP signaling pathway plays an important role in signal transduction for certain pheromones and MHC peptides (16, 19–21). However, the potential involvement of other signaling pathways is not fully understood (21, 22).

Previously, we demonstrated that genetic elimination of subunit A2 of the CNG channel, which disrupts the canonical cAMP pathway, significantly reduced but did not eliminate physiological and behavioral responses to pheromones in the main olfactory system (22). The transduction pathway responsible for these responses was not identified, but pharmacological experiments suggested involvement of phospholipase C (PLC). In this study, we sought to find whether transient receptor potential (TRP) channels, known effectors of the PLC pathway involved in sensory signaling (23), are involved in olfactory transduction. Below, we describe expression of TRP channel M5 (TRPM5), a member of the melastatin-related TRP channel family in the MOE, and implicate a role for this channel in pheromone transduction.

Results

GFP Expression Driven by the TRPM5 Promoter in the MOE. In transgenic mice, where the TRPM5 promoter drives expression of GFP (TRPM5-GFP mice), we found GFP expression in two morphologically distinct populations of cells in the MOE (Fig. 1*A*). Cells in one population were short (usually <15 μm), and their cell bodies were located in the superficial (apical) layer, where the nuclei of sustentacular cells are found (Fig. 1*A*, arrowheads, and *Inset a*). Features of these cells include apical microvillus-like processes and absence of apparent basal axonal processes. These cells belong to a unique population of microvillar-like cells whose characteristics will be described in detail elsewhere (data not shown). The microvillar-like cells were expressed sparsely throughout the olfactory epithelium [Fig. 1*A* and supporting information (SI) Fig. 6] and constituted a small fraction of the total number of GFP-labeled cells.

Author contributions: W.L., R.M., and D.R. designed research; W.L. and G.D. performed research; R.M. and S.W.H. contributed new reagents/analytic tools; W.L., G.D., S.W.H., and D.R. analyzed data; and W.L. and D.R. wrote the paper.

The authors declare no conflict of interest.

This article is a PNAS direct submission.

Abbreviations: OSN, olfactory sensory neuron; TRPM5, transient receptor potential channel M5; CNG, cyclic nucleotide-gated; CNGA2, CNG channel subunit A2; AC, adenylyl cyclase; MOE, main olfactory epithelium; PLC, phospholipase C; TRP, transient receptor potential; STED, stimulated emission depletion; OMP, olfactory marker protein; DMP, 2,5-dimethylpyrazine; MTMT, (methylthio)methanethiol; EOG, electroolfactogram; SQ22536, 9-(tetrahydro-2-furyl)-adenine.

¶To whom correspondence should be addressed at: Department of Cell and Developmental Biology, University of Colorado at Denver and Health Sciences Center at Fitzsimons, Mail Stop 8108, Building RC1, Room L18-11119, 12801 East 17th Avenue, P.O. Box 6511, Aurora, CO 80045. E-mail: diego.restrepo@uchsc.edu.

This article contains supporting information online at www.pnas.org/cgi/content/full/0610201104/DC1.

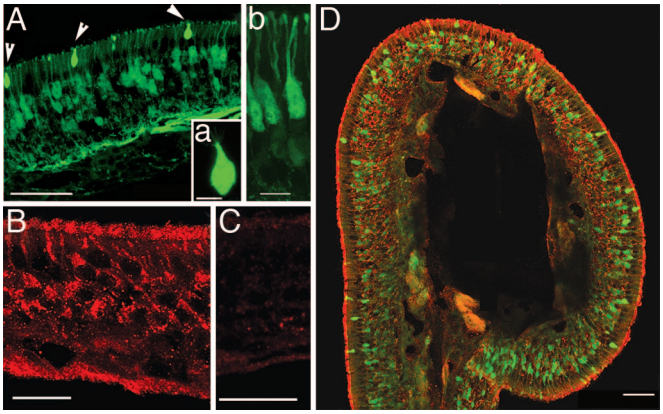

Fig. 1. TRPM5 promoter-driven GFP and TRPM5-like antigenicity in the MOE. (*A*) TRPM5 promoter drove GFP expression in two populations of cells with distinct morphology: sparsely distributed short cells <15 μm in length (arrowheads and *Inset a*) and densely packed OSNs (representative OSNs are shown in *Inset b*). (*B*) A representative confocal image showing immunolabel for TRPM5 at a higher magnification. (*C*) Negative control, image taken from an olfactory epithelium section from a TRPM5 knockout mouse labeled with the anti-TRPM5 antibody. (*D*) OSNs expressing GFP in TRPM5-GFP mice (green) also displayed immunoreactivity for TRPM5 (red). (Scale bars: *A*, *B*, and *C*, 20 μm; *Inset a*, 5 μm; *Inset b*, 10 μm; *D*, 50 μm.)

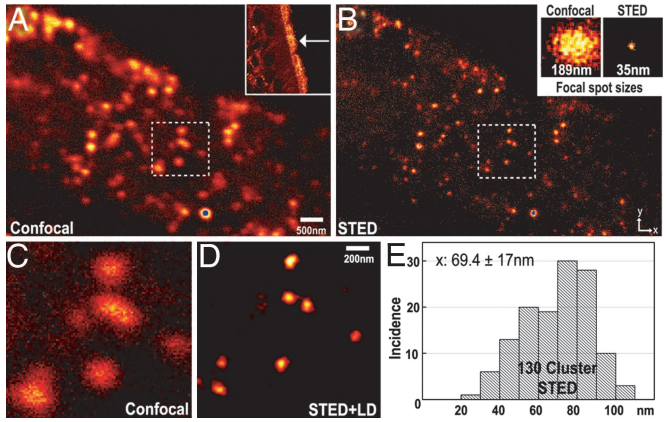

Fig. 2. Analysis of spot size for STED images of TRPM5 immunoreactivity in the cilia layer. (*A* and *B*) Confocal (*A*) and STED (*B*) images of TRPM5 immunofluorescence in the cilia layer of the olfactory epithelium. (*A Inset*) Confocal image at a lower magnification taken with a confocal microscope. (*B Inset*) Smallest spot gained from the faintest antibody cluster observed in the sample is indicative of the maximum size of the effective point-spread function in the confocal (189-nm) and STED (35-nm) imaging modes. (*C* and *D*) Higher-magnification images of the areas enclosed by the dashed boxes in *A* and *B*, respectively. The image in *D* is the STED image after a linear deconvolution (LD). (*E*) Histogram showing the distribution of full width at half maxima (FWHM) for the clusters in three separate images (130 individual clusters from three separate images). To estimate the FWHM, background was subtracted from the STED images, and each cluster was fit with Lorentz-shaped profiles.

In contrast, most of the GFP-positive cells resembled bipolar olfactory sensory neurons (OSNs) (Fig. 1*A Inset b*). These cells extended an apical dendritic process to the luminal surface of the epithelium. OSNs expressing GFP bear axon-like processes that reached below the basal lamina, where they joined axon bundles that projected to the olfactory bulb (Fig. 1*A*). Interestingly, these presumed OSNs were not distributed homogeneously throughout the olfactory epithelium, being more abundant in the ventrolateral zones of the MOE (SI Fig. 6).

TRPM5 Antibody Labels a Subset of OSNs. TRPM5-like immunofluorescence was seen in both apical processes and soma of OSNs with dense labeling in the olfactory knobs and the cilia layer, where signal transduction is thought to occur (Fig. 1 *B–D*). When the antibody was used in sections from the TRPM5-GFP mice (n = 4), we found immunoreactivity in GFP-expressing cells (Fig. 1*D*). Occasionally, immunolabeling of the TRPM5 antibody was found in areas with weak GFP expression (data not shown). As a control, olfactory epithelium sections from a mouse in which the TRPM5 coding region was eliminated did not show any immunoreactivity (Fig. 1*C*).

To obtain high-resolution images of TRPM5 antibody immunolabeling in the apical layer, we used stimulated emission depletion (STED) microscopy, a unique type of fluorescence microscopy that allowed us to obtain a resolution of <35 nm, significantly below the diffraction-limited resolution of other light microscopes (24, 25). Fig. 2 *A* and *B* shows high-magnification confocal (*A*) and STED (*B*) images of the apical layer of the olfactory epithelium stained with TRPM5 antibody (Fig. 2*A Inset*). Higher magnification images of the areas enclosed by the dashed boxes in Fig. 2 *A* and *B*, respectively, are shown in Fig. 2 *C* and *D*. We found that the antibody labeled discrete spots with an average size of 69 nm (Fig. 2*E*). We found a similar punctate distribution for CNGA2 (data not shown), consistent with previous electron microscopy studies (26).

Expression of TRPM5 in Mature OSNs. To determine whether mature OSNs express TRPM5, we performed double-label experiments with antibodies against TRPM5 and olfactory marker protein (OMP), a marker for mature OSNs (Fig. 3 *A–C*). Many OMP-positive OSNs also were TRPM5-positive (Fig. 3*A*). In sections cut through the olfactory epithelium, there was considerable overlap of expression of TRPM5 and OMP in the proximal cilia layer, and the overlap decreased at the distal end. In sections cut perpendicular to the apical end of the dendrites, OMP labeled numerous cilia and dendritic knobs. Colocalization of OMP and TRPM5 is apparent, especially in the dendritic knobs and the base of the cilia (Fig. 3*B*). In TRPM5-GFP mice, axons from the TRPM5-expressing cells also were GFP-positive, allowing us to identify glomeruli targeted by TRPM5-expressing OSNs. We found coexpression of OMP and GFP in GFP-positive glomeruli in the olfactory bulb of TRPM5-GFP mice. Together, these data demonstrate the expression of TRPM5 in a subset of mature OSNs in the MOE.

Coexpression of TRPM5 and CNGA2. The large number of TRPM5-expressing OSNs in the MOE suggested that TRPM5 may be present in the cells expressing elements of the canonical cAMP pathway. Using immunofluorescence with an antibody against CNGA2 in sections of TRPM5-GFP mice, we examined the potential coexpression of the two ion channels. As shown in Fig. 3*D*, CNGA2 antibody labeled a majority of OSNs. The reactivity was intense in the cilia layer as reported in ref. 27. Weaker, but evident, immunoreactivity for the CNGA2 antibody was found in the soma. GFP was present in many of the CNGA2-expressing cells, suggesting that TRPM5 and CNGA2 were coexpressed in many OSNs (Fig. 3*D*). A few OSNs appeared to express GFP in the absence of CNGA2. Consistent with these findings, the majority of GFP-positive glomeruli in TRPM5-GFP mice also stained for CNGA2, which is known to be expressed in OSN axons (Fig. 3*E*).

Coexpression of TRPM5 and Components of the PLC Pathway. In taste receptor cells, G protein β and γ13 subunits activate PLC β2 (28), resulting in activation of TRPM5 (29). To investigate whether the PLC pathway is present in OSNs, we immunoreacted sections from TRPM5-GFP mice with antisera against PLC β2 and γ13. The anti-PLC β2 antibody labeled the majority of OSNs. Strong reaction was observed in the axon bundles

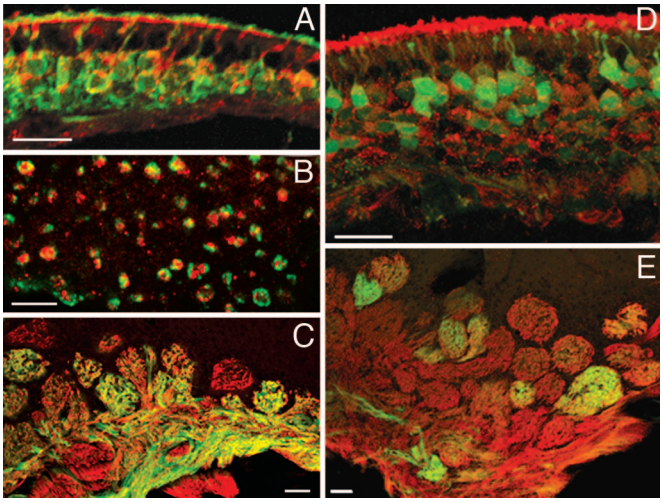

Fig. 3. Colocalization of TRPM5 or GFP immunostaining with OMP or CNGA2 immunoreactivity. (*A*) OMP immunoreactivity (green) was seen in mature OSNs. A subset also labeled with TRPM5 antibody (red). (*B*) A confocal image from a section cut perpendicular to the dendrites at the level of the dendritic knobs and cilia displays immunolabel for OMP and TRPM5. (*C*) Sagittal image of the ventral portion of the olfactory bulb of a TRPM5-GFP mouse. Axons from TRPM5-expressing OSNs (green) project to a subset of glomeruli that were immunopositive for OMP (red, overlap appears as yellow). (*D*) An antibody against CNGA2 (red) labeled the apical layer and soma of the majority of OSNs in a TRPM5-GFP mouse. GFP (green) was present in many such OSNs, an indication of coexpression of these ion channels. (*E*) Immunoreactivity for CNGA2 (red) and GFP (green) in the ventral olfactory bulb (saggital section) in a TRPM5-GFP mouse. Most of the GFP-positive glomeruli also were immunoreactive for CNGA2. A relatively small number of glomeruli displayed GFP expression but stained weakly for CNGA2. (Scale bars: *A* and *D*, 20 μm; *B*, 5 μm; *C* and *E*, 50 μm.)

(SI Fig. 7*A*). As shown in a higher magnification fluorescence micrograph (SI Fig. 7*B*) GFP was present in PLC β2-positive OSNs, suggesting colocalization of TRPM5 and PLC β2. Similarly, immunoreactivity for the γ13 was present in GFP-positive OSNs (SI Fig. 7 *C* and *D*).

Axonal Projections of the TRPM5-Expressing OSNs. Given that we detected expression of GFP predominantly in the ventrolateral areas of the olfactory epithelium, we expected differential location of GFP-positive glomeruli in the olfactory bulb because axonal connection between the MOE and the olfactory bulb follows a basic principle of "zone-to-zone projection" (30). Fig. 4 *A* and *B* shows discrete expression of GFP in spatially segregated glomeruli in the medial and lateral surfaces of whole-mount olfactory bulb in TRPM5-GFP mice. Glomeruli in the ventral surface cannot be seen clearly in whole mount because of fluorescence in the nerve layer. To chart expression throughout the glomerular layer, we stained with an antibody against GFP in transverse serial sections (Fig. 4 *C–E*). A representative section is shown in Fig. 4*C*, a representative 2D map is shown in Fig. 4*D*, and the average glomerular density map for six mice is shown in Fig. 4*E*. Large numbers of GFP-positive glomeruli were located at the ventral regions along the rostral–caudal axis. In addition, many GFP-positive glomeruli were seen in anterior-medial and posterior-lateral areas of the bulb. There were 520 ± 149 GFP-positive glomeruli (mean ± SD, $n = 6$, range 353–750, corrected for oversampling) with an average diameter of 94 ± 5 μm. We found that TRPM5-expressing OSNs targeted both regular and microglomeruli (31). These results demonstrate that TRPM5-expressing OSNs preferentially project discreet areas of the bulb, consistent with the zonal expression of TRPM5 in the MOE.

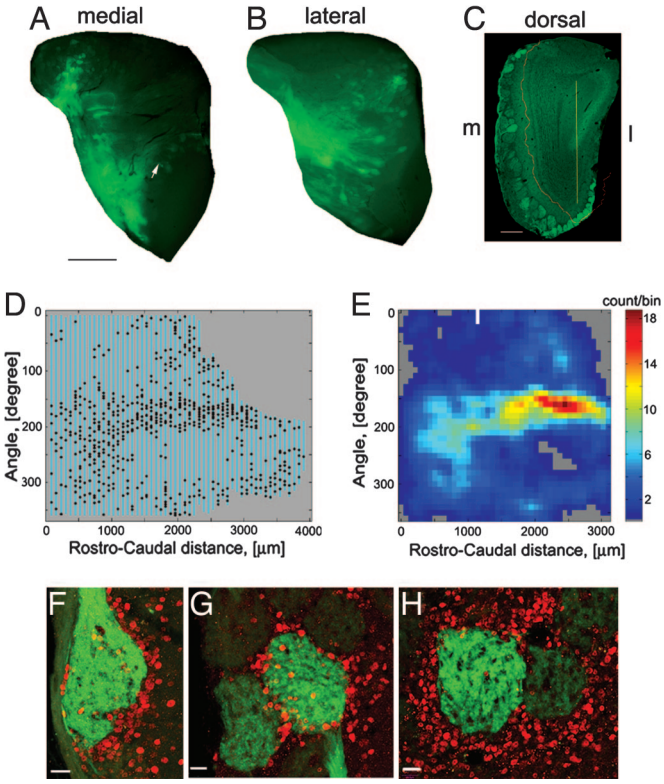

Fig. 4. Glomeruli targeted by TRPM5-expressing OSNs were detected as GFP-positive glomeruli in TRPM5-GFP mice. (*A* and *B*) Whole-mount images showing GFP-positive axons and targeted glomeruli in medial (*A*) and lateral (*B*) surfaces of the olfactory bulb. (*C*) A transverse section showing GFP-positive glomeruli. A line drawn through the subventricular zone is the axis used to map glomeruli in *D* and *E*. m, medial; l, lateral. (*D*) A representative 2D map showing location of GFP-positive glomeruli along the rostrocaudal distance and angle around the transverse section. (*E*) A pseudocolor rendering of the average number of glomeruli in bins of 10° and 72 μm (average from six bulbs), showing that the highest density of GFP-positive glomeruli was located in the ventral region of the bulb. (*F–H*) Representative glomeruli that were activated by the pheromone DMP (*F*), the sex-specific odorant MTMT (*G*), and soiled bedding from a mating pair (*H*). Activated glomeruli were identified by numerous Fos-expressing periglomerular neurons (red). GFP antibody immunohistochemistry was used in *C* and *F–H*. (Scale bars: *A* and *B*, 1 mm; *C*, 100 μm; *F–H*, 20 μm.)

Activation of the GFP-Positive Glomeruli. The localization of the TRPM5-GFP-positive glomeruli in the ventral area of the olfactory bulb was intriguing because this area overlaps with domains responsive to mouse urine and putative pheromones (22, 32–34) (see SI Movie 1). To determine whether the TRPM5-GFP-positive glomeruli respond to these semiochemicals, we surveyed odor responsiveness of glomeruli by detecting neuronal activity-dependent Fos protein expression in the periglomerular cells surrounding glomeruli. Exposure to the putative pheromone 2,5-dimethylpyrazine (DMP) (35), the social attractant (methylthio)methanethiol (MTMT) (34), mouse urine, and soiled bedding from a mating pair all resulted in activation of many GFP-positive glomeruli as measured by Fos expression in periglomerular cells (Fig. 4 *F–H*, mouse urine not shown). Exposure to fresh air or lilial did not produce similar activation patterns in the GFP-positive glomeruli. The data indicated that the glomeruli targeted by TRPM5-expressing OSNs respond to semiochemicals in the ventral area, where we previously demonstrated activation by putative pheromones and urine.

Electroolfactogram (EOG) Responses in TRPM5 Knockout Mice. TRPM5 knockouts did not show obvious deficits in body weight, reproduction, and performance on a go/no go olfactory detec-

NEUROSCIENCE

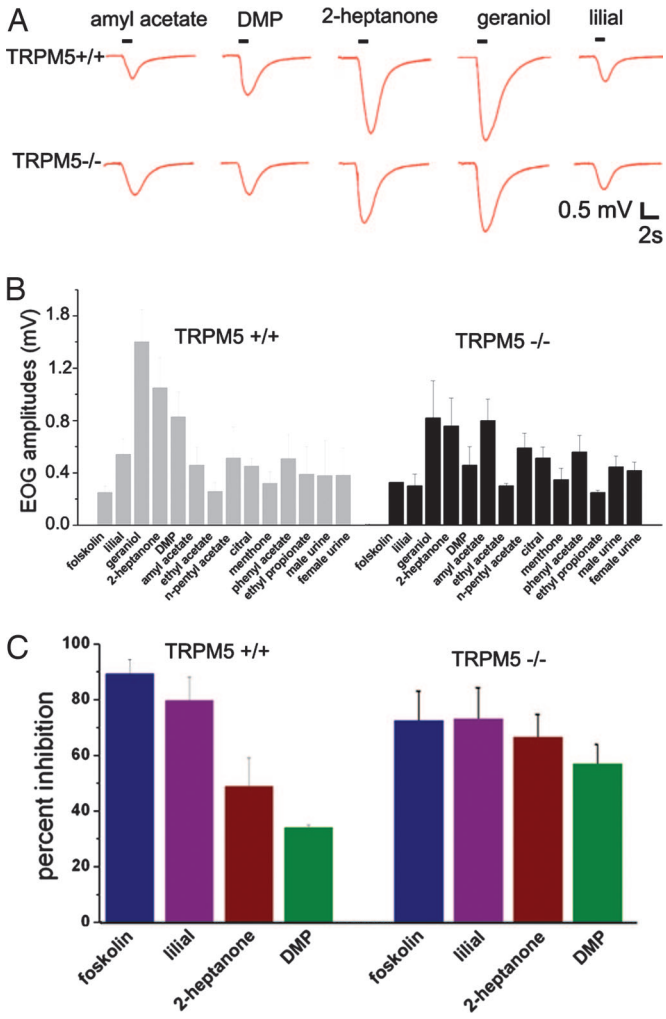

Fig. 5. EOG recordings from wild-type (TRPM5 +/+) and TRPM5 knockout (TRPM5 −/−) mice. (*A*) Representative EOG traces. (*B*) Average peak EOG responses to different odors ($n = 4–12$). There was no significant difference between knockout and control ($P < 0.7$ for ANOVA). All odorants were presented at 100 μM in Ringer's, and forskolin was presented at a concentration significantly below saturation (20 μM). A 1 mM concentration of 3-isobutyl-1-methylxanthine (IBMX) elicited a saturating response (≈4 mV; data not shown). (*C*) In wild-type mice, the ACIII inhibitor SQ33256 (300 μm) suppressed EOG responses induced by forskolin (an ACIII activator) and lilial to a larger extent than responses induced by the pheromones 2-heptanone and DMP ($n = 4$). This differential inhibition disappeared in the knockout animals. A mixed ANOVA with mouse strain and odor as fixed factors and mouse as a random effect yielded a P value of 0.036 for a strain–odor interaction. Post hoc Tukey–Kramer tests showed that the difference in inhibition between forskolin or lilial and the pheromones DMP and 2-heptanone is not significant in the knockouts (post hoc P values >0.05 in the knockout and <0.05 in the controls). Error bars are SEM.

tion task (data not shown). In EOG recordings monitoring odor-evoked field potentials in the MOE, TRPM5 knockout mice responded to all of the odorants tested (Fig. 5 *A* and *B*). There was no statistical difference in EOG responses between wild-type and TRPM5 knockout mice (Fig. 5*B*). This finding was not unexpected given that the dominant cAMP pathway is functional and is expressed in the TRPM5-positive OSNs.

Previously, we have shown that in wild-type mice the degree of suppression of EOG responses by the AC inhibitor 9-(tetrahydro-2-furyl)-adenine (SQ22536) is larger for forskolin and environmental odorants (lilial and geraniol) as compared with suppression of EOG responses elicited by the putative pheromones 2-heptanone and DMP (22). In contrast, the same degree of suppression of EOG responses was obtained for forskolin, environmental odorants, and pheromones when SQ22536 was presented in the presence of the PLC inhibitor U73122. The effect of U73122 suggested that the PLC pathway is involved. We reasoned that if TRPM5 participates in PLC signal transduction to putative pheromones, the genetic excision of TRPM5 should eliminate the differential inhibition of pheromone-induced EOG by SQ22536. Fig. 5*C* shows that the differential inhibition of odorant-induced versus pheromone-induced EOG by SQ22536 is absent in the TRPM5 knockout. Thus, in control mice, the post hoc P value for forskolin versus DMP is 0.001 and for forskolin versus heptanone it is 0.03. This contrasts with P values in TRPM5 knockouts of 0.67 for forskolin versus DMP and 0.66 for forskolin versus heptanone. This result indicates that TRPM5 participates in signal transduction for putative pheromones consistent with olfactory bulb activation of TRPM5-positive glomeruli by DMP (Fig. 5*H*) and responsiveness of CNGA2 knockout mice to pheromones (22).

Discussion

We find that TRPM5 is expressed in a subset of OSNs. Axons of these OSNs predominantly project to glomeruli in the ventral olfactory bulbs, regions known to process semiochemicals. Indeed, we observed that the targeted glomeruli were activated by pheromones, social attractants, and soiled bedding from mating pairs. Thus, TRPM5 participates in chemosensory transduction, not only in the taste system, as previously reported (29, 36), but also in the olfactory system.

Our finding strengthens the increasingly important role for TRP channels in chemical sensing. A TRP-like channel has been identified in physiological experiments in lobster OSNs (37), TRPC2 has been postulated to mediate chemical detection in the vomeronasal organ (12, 14), and TRPC6 is found in a subset of odor-responsive cells in the olfactory epithelium (38). The TRPC6-expressing cells do not express OMP and are morphologically distinct from the OMP-expressing TRPM5 OSNs described here. In addition, TRPA1 responds to pungent chemical stimuli, TRPV1 responds to the hot chili pepper irritant capsaicin, and TRPM8 responds to menthol and the cooling agent icilin (23). Finally, the role of TRP channels in chemosensory transduction is conserved phylogenetically because a TRPV channel plays a role in olfaction in *Caenorhabditis elegans* (39).

An intriguing finding is the coexpression of TRPM5 and CNGA2 in the majority of TRPM5-expressing OSNs, suggesting interplay between the canonical cAMP and the PLC pathway. Could these two channels interact directly? TRPM5 is a Ca^{2+}-activated channel (40, 41), whereas, under physiological conditions, the current flowing through CNGA2 is made up mostly of Ca^{2+} (42). Intriguingly, the finding that immunoreactivity for TRPM5 is found in small spots with an average diameter of 69 nm suggests that these channels may be clustered in small microdomains. If CNGA2 and TRPM5 were colocalized, there would be efficient activation of the TRPM5 channel by Ca^{2+} flowing through the CNGA2 channel. This is a possibility that must be explored in future high-resolution microscopy experiments. Alternately, TRPM5 may be regulated through activation of PLC by G protein β and γ subunits, resulting in an increase of the second messenger inositol 1,4,5-trisphosphate ($InsP_3$) that would release Ca^{2+} from internal stores, a mechanism that has been proposed for the taste system (29, 36). Indeed, there are reports of expression of $InsP_3$ receptor in subsets of cells in the olfactory epithelium (43), and we observe immunoreactivity for PLC β2 and γ13 in the MOE (SI Fig. 7).

We found that TRPM5 was expressed preferentially by OSNs located in the ventrolateral zones of the olfactory epithelium. As expected from the basic principle of zone-to-zone projection (30) between the olfactory epithelium and bulb, the majority of the

glomeruli innervated by TRPM5-expressing OSNs were found in ventral regions of the olfactory bulb. The same area of the bulb is known to be activated by urine and putative pheromones (22, 32–34). Consistent with these observations, we find that the ventral glomeruli formed by axons from TRPM5-expressing OSNs respond to semiochemicals. Together, the published studies on the chemosensory responsiveness of this area of the bulb and our observations suggest that, as postulated on a cryoarchitectonic basis,[‖] this ventromedial/ventrolateral area of the olfactory bulb may constitute an "olfactory fovea" critical in processing information on semiochemicals, including urine. A question raised by these observations is whether the ventral areas of the olfactory bulb process sensory signals differently from the dorsal areas.

Previously, we found that genetic deletion of CNGA2 dramatically reduced but did not eliminate pheromone-induced EOG responses and the number of pheromone-activated glomeruli in the main olfactory bulb (22). Interestingly, the majority of the glomeruli that were no longer activated by pheromones in the CNGA2 knockout mice were located in the dorsal region, and responsiveness in the ventral area, where TRPM5 glomeruli are found, was relatively spared (22). Both CNGA2 knockout male and female mice housing continually with opposite genders, respectively, produce smaller number of pups per litter (data not shown). It is likely that TRPM5 participates in pheromone transduction in the CNGA2-defective mouse and that, in wild-type mice, TRPM5 has a role in transduction and interacts with the canonical cAMP pathway in sensing semiochemicals, particularly in OSNs that send axons to the ventral regions of olfactory bulbs.

Materials and Methods

Animals. TRPM5-GFP and TRPM5 knockout mice (44, 45) were bred in-house in University of Colorado at Denver and Health Sciences Center. The PCR was used to genotype the mice based on absence of the deleted coding region of TRPM5 and presence of the neomycin resistance gene. C57BL/6 mice were used in other experiments. Animals were 3–8 months old. All procedures were in compliance with the University of Colorado at Denver and Health Sciences Center Animal Care and Use Committee.

Odorants and Other Chemicals. Odorants were obtained from Aldrich Chemical Co. (Milwaukee, WI), Fluka (Ronkon Koma, NY), or Takasago Corporation (Shinagawa, Japan). Odorants were either made freshly by dilution with vigorous vortexing and sonication into water (for odor exposure in Fos experiments) or made in Ringer's saline containing 145 mM NaCl, 5 mM KCl, 20 mM *N*-2-hydroxyethylpiperazine-*N*′-2-ethanesulfonic acid buffer-Hepes, 1 mM $MgCl_2$, 1 mM $CaCl_2$, 1 mM Na pyruvate, and 5 mM D-glucose (pH 7.2) (for EOG recordings). The AC activator forskolin and the AC inhibitor SQ22536 were purchased from Calbiochem (San Diego, CA).

EOG Recordings. The EOG recordings were performed as described in ref. 46 with slight modifications. Briefly, mice were killed by CO_2 inhalation followed by cervical dislocation. The head was split along the midline, and the nasal septum was removed to expose the endoturbinates. Turbinates III and IV were removed to expose the olfactory epithelium lining the exoturbinates. The half-head was mounted on a recording chamber by using the dental adhesive Impregum F (ESPE, Neuss, Germany). For experiments probing inhibition of EOG responses by the AC blocker SQ22536, the turbinates were incubated with the inhibitor for 10–15 min to ensure equilibration across the apical membrane. A concentration of 300 μM SQ22536 was chosen because it yields near maximal suppression of forskolin responses while inhibiting only a small fraction of the responses to 2-heptantone and DMP (22). These conditions are optimal for detecting differences between TRPM5 knockouts and controls. A mixed-model ANOVA run by using PROC MIXED in SAS (47) was used to determine whether there were differences between TRPM5 knockouts and controls in Fig. 5*C*. Strain and odor were entered as fixed effects, and mouse was entered as a random effect.

Detection of Odor-Induced Fos Expression in Periglomerular Cells. DMP (0.01%) was made up freshly in 25 ml of water. TRPM5-GFP mice were placed in a plastic chamber with fresh air continuously flowing at 1,950 ml/min. A MATLAB (MathWorks, Natick, MA) program controlled the delivery of odor-equilibrated air stream at 50 ml/min to the chamber, producing odor stimulus with 40 times dilution of the original concentration. Mice were exposed to fresh air in the chamber for 90 min before being exposed to odorants. Odorant exposure occurred intermittently to minimize adaptation effects. Odors were presented six times for 2 min with 3-min intervening fresh air intervals over a 30-min period. The mouse remained in the same chamber under constant perfusion with fresh air for 1 h and 15 min before euthanasia. For exposure to MTMT or soiled bedding of a mating pair, individual mice were transferred to a clean cage and adapted for 2 h. A total of 25 μl of MTMT (50 ppm) or a scoop of soiled bedding was added to the cage. Mice were allowed to sample the stimuli freely for 1.5 h before they were euthanized.

Tissue Preparation for Immunolabeling. For euthanasia, mice were anesthetized with ketamine/xylazine (20–100 μg/g of body weight), perfused transcardially with 0.1 M phosphate buffer (PB) followed by a PB-buffered fixative containing 3% paraformaldehyde, 0.019 M L-lysine monohydrochloride, and 0.23% sodium *m*-periodate (22). The olfactory bulbs and nose were harvested and postfixed for 2 h before being transferred for cryoprotection into PBS with 25% sucrose overnight. Olfactory bulbs were either cryosectioned sagittally into free-floating 30-μm-thick sections or cut into 18-μm-thick transverse sections mounted on Superfrost Plus slides (VWR, West Chester, PA) (for olfactory bulb mapping experiments). Sections used for STED were 4-μm-thick to minimize light scattering and background fluorescence. Sagittal cuts maximized the number of glomeruli visualized in medial and lateral sections.

For immunolabeling, sections were rinsed and incubated in blocking solution containing 2% normal donkey serum, 0.3% Triton X-100, and 1% BSA in PBS for 1.5 h. Sections then were incubated with primary antibodies for periods from overnight to 72 h. Antibodies against the following proteins were used: rabbit anti-Fos (1:10,000; Oncogen, Boston, MA), rabbit anti-TRPM5 (1:250 or 1:500) (48), rabbit anti-CNGA2 (1:200; Alomone Labs Ltd., Jerusalem, Israel), goat anti-OMP [1:6,000; kindly provided by Frank Margolis, University of Maryland, School of Medicine, Baltimore, MD (49)], chick anti-GFP (1:2,000, Chemicon, Temecula, CA), and PLCβ2 (1:200; Santa Cruz, CA). After incubation with the primary antibodies, sections were washed and reacted with conjugated secondary antibodies (Molecular Probes, Eugene, OR) for 1 h at room temperature. Secondary antibodies included donkey anti-rabbit or goat conjugated Alexa 555 (Molecular Probes) and donkey anti-chicken conjugated with FITC. Sections then were rinsed and mounted on slides with Fluoromount-G (Fisher Biotech, Birmingham, AL). For STED, we used ATTO 532 anti-rabbit as the secondary antibody (Atto-Tech, Siegen, Germany). Removal of primary antibody resulted in no labeling in control sections. Confocal images were

[‖]Meisami, E., Emaiman, S. (1985) *Chem. Senses* Vol. 10, p. 375 (abstr.).

obtained by using an Olympus (Center Valley, PA) Fluoview 300 microscope.

STED Microscopy. STED microscopy was performed as detailed in ref. 50. Briefly, the fluorophore (anti-rabbit IgG labeled with ATTO 532) was stimulated in a diffraction-limited spot by a laser diode (Picoquant, Berlin, Germany) emitting ≈80-ps pulses at 470 nm at a rate of 0.25 Mhz. The excitation pulse was followed by a doughnut-shaped 200-ps pulse of light tuned to a specific wavelength used for STED generated by a Ti-Sapphire laser and modulated by an optic parametric amplifier (Coherent, Santa Clara, CA). Under the applied conditions of operation, use of STED resulted in a resolution <35 nm (50) in the sample. Detection was accomplished by a counting avalanche photodiode (Perkin–Elmer Optoelectronics, Fremont, CA). The image was generated by scanning the sample with a 5-nm resolving piezo stage operating in the closed loop (Melles Griot, Cambridge, U.K.). A single-step linear deconvolution (Wiener filter) was carried out with the point-spread function of the STED microscope.

Mapping of GFP-Positive Glomeruli in Olfactory Bulbs of TRPM5-GFP Mice. We used a mapping method and software developed in our laboratory (51, 52) as described in detail in the *SI Text*.

We thank Steven Glidewell for technical help, Drs. Ernesto Salcedo and Eugene Kronberg for support with main olfactory bulb mapping, Drs. Thomas Finger and Emily Liman for discussion, Dr. Gary Zerbe for advice on statistics, Dr. Lawrence Katz (Duke University Medical Center, Durham, NC) for the gift of MTMT, and Dr. Frank Margolis for the gift of OMP antibody. The work was funded by National Institutes of Health Grants DC00566, DC004657, and DC006070 (to D.R.), DC03055 and DC03155 (to R.M.), and DC006828 (to W.L.) and by an Exzellenzfond grant from the Max Planck Society (to S.W.H.).

1. Restrepo D, Arellano J, Oliva AM, Schaefer ML, Lin W (2004) *Horm Behav* 46:247–256.
2. Ache BW, Young JM (2005) *Neuron* 48:417–430.
3. Shepherd GM (2006) *Nature* 439:149–151.
4. Brennan PA, Zufall F (2006) *Nature* 444:308–315.
5. Schild D, Restrepo D (1998) *Physiol Rev* 78:429–466.
6. Gold GH (1999) *Annu Rev Physiol* 61:857–871.
7. Brunet LJ, Gold GH, Ngai J (1996) *Neuron* 17:681–693.
8. Belluscio L, Gold GH, Nemes A, Axel R (1998) *Neuron* 20:69–81.
9. Wong ST, Trinh K, Hacker B, Chan GC, Lowe G, Gaggar A, Xia Z, Gold GH, Storm DR (2000) *Neuron* 27:487–497.
10. Boehm T, Zufall F (2006) *Trends Neurosci* 29:100–107.
11. Dulac C, Wagner S (2006) *Annu Rev Genet* 40:449–467.
12. Dulac C, Torello AT (2003) *Nat Rev Neurosci* 4:551–562.
13. Restrepo D, Lin W, Salcedo E, Yamazaki K, Beauchamp GK (2006) *Trends Neurosci* 29:604–609.
14. Halpern M, Martinez-Marcos A (2003) *Prog Neurobiol* 70:245–318.
15. Baxi KN, Dorries KM, Eisthen HL (2006) *Trends Neurosci* 29:1–7.
16. Yoon H, Enquist LW, Dulac C (2005) *Cell* 123:669–682.
17. Boehm U, Zou Z, Buck LB (2005) *Cell* 123:683–695.
18. Liberles SD, Buck LB (2006) *Nature* 442:645–650.
19. Spehr M, Kelliher KR, Li XH, Boehm T, Leinders-Zufall T, Zufall F (2006) *J Neurosci* 26:1961–1970.
20. Mandiyan VS, Coats JK, Shah NM (2005) *Nat Neurosci* 8:1660–1662.
21. Wang Z, Balet SC, Li V, Nudelman A, Chan GC, Storm DR (2006) *J Neurosci* 26:7375–7379.
22. Lin W, Arellano J, Slotnick B, Restrepo D (2004) *J Neurosci* 24:3703–3710.
23. Clapham DE, Julius D, Montell C, Schultz G (2005) *Pharmacol Rev* 57:427–450.
24. Donnert G, Keller J, Medda R, Andrei MA, Rizzoli SO, Luhrmann R, Jahn R, Eggeling C, Hell SW (2006) *Proc Natl Acad Sci USA* 103:11440–11445.
25. Hell SW, Wichmann J (1994) *Opt Lett* 19:780–782.
26. Matsuzaki O, Bakin RE, Cai X, Menco BP, Ronnett GV (1999) *Neuroscience* 94:131–140.
27. Dhallan RS, Yau KW, Schrader KA, Reed RR (1990) *Nature* 347:184–187.
28. Huang L, Shanker YG, Dubauskaite J, Zheng JZ, Yan W, Rosenzweig S, Spielman AI, Max M, Margolskee RF (1999) *Nat Neurosci* 2:1055–1062.
29. Zhang Y, Hoon MA, Chandrashekar J, Mueller KL, Cook B, Wu D, Zuker CS, Ryba NJ (2003) *Cell* 112:293–301.
30. Mori K, Nagao H, Yoshihara Y (1999) *Science* 286:711–715.
31. Lipscomb BW, Treloar HB, Greer CA (2002) *J Neurosci* 22:766–774.
32. Xu F, Schaefer M, Kida I, Schafer J, Liu N, Rothman DL, Hyder F, Restrepo D, Shepherd GM (2005) *J Comp Neurol* 489:491–500.
33. Schaefer ML, Yamazaki K, Osada K, Restrepo D, Beauchamp GK (2002) *J Neurosci* 22:9513–9521.
34. Lin dY, Zhang SZ, Block E, Katz LC (2005) *Nature* 434:470–477.
35. Novotny MV (2003) *Biochem Soc Trans* 31:117–122.
36. Perez CA, Huang L, Rong M, Kozak JA, Preuss AK, Zhang H, Max M, Margolskee RF (2002) *Nat Neurosci* 5:1169–1176.
37. Bobkov YV, Ache BW (2005) *J Neurophysiol* 93:1372–1380.
38. Elsaesser R, Montani G, Tirindelli R, Paysan J (2005) *Eur J Neurosci* 21:2692–2700.
39. Kahn-Kirby AH, Bargmann CI (2006) *Annu Rev Physiol* 68:719–736.
40. Liu D, Liman ER (2003) *Proc Natl Acad Sci USA* 100:15160–15165.
41. Prawitt D, Monteilh-Zoller MK, Brixel L, Spangenberg C, Zabel B, Fleig A, Penner R (2003) *Proc Natl Acad Sci USA* 100:15166–15171.
42. Frings S, Seifert R, Godde M, Kaupp UB (1995) *Neuron* 15:169–179.
43. Cunningham AM, Ryugo DK, Sharp AH, Reed RR, Snyder SH, Ronnett GV (1993) *Neuroscience* 57:339–352.
44. Damak S, Rong M, Yasumatsu K, Kokrashvili Z, Perez CA, Shigemura N, Yoshida R, Mosinger B, Jr, Glendinning JI, Ninomiya Y, *et al.* (2006) *Chem Senses* 31:253–264.
45. Clapp TR, Medler KF, Damak S, Margolskee RF, Kinnamon SC (2006) *BMC Biol* 4:7.
46. Schaefer ML, Young DA, Restrepo D (2001) *J Neurosci* 21:2481–2487.
47. SAS Institute Inc (2004) *SAS OnlineDoc 9.1.3* (SAS Institute Inc, Cary, NC), http://support.sas.com/onlinedoc/913/docMainpage.jsp.
48. Perez CA, Margolskee RF, Kinnamon SC, Ogura T (2003) *Cell Calcium* 33:541–549.
49. Verhaagen J, Oestreicher AB, Gispen WH, Margolis FL (1989) *J Neurosci* 9:683–691.
50. Donnert G, Keller J, Medda R, Andrei MA, Rizzoli SO, Luhrmann R, Jahn R, Eggeling C, Hell SW (2006) *Proc Natl Acad Sci USA* 103:11440–11445.
51. Schaefer ML, Finger TE, Restrepo D (2001) *J Comp Neurol* 436:351–362.
52. Salcedo E, Zhang C, Kronberg E, Restrepo D (2005) *Chem Senses* 30:615–626.